

Macroscopic maximally-entangled-state preparation between two atomic ensemblesManish Chaudhary ^{1,2,*}, Ebubechukwu O. Ilo-Okeke ^{2,3}, Valentin Ivannikov^{2,4} and Tim Byrnes^{2,1,4,5,6,7,†}¹*State Key Laboratory of Precision Spectroscopy, School of Physical and Material Sciences, East China Normal University, Shanghai 200062, China*²*New York University Shanghai, 567 West Yangsi Road, Pudong, Shanghai 200126, China*³*Department of Physics, School of Physical Sciences, Federal University of Technology, P. M. B. 1526, Owerri, Imo State 460001, Nigeria*⁴*NYU-ECNU Institute of Physics at NYU Shanghai, 3663 Zhongshan Road North, Shanghai 200062, China*⁵*Center for Quantum and Topological Systems (CQTS), NYUAD Research Institute, New York University, Abu Dhabi 129188, United Arab Emirates*⁶*Shanghai Frontiers Science Center of Artificial Intelligence and Deep Learning, 567 West Yangsi Road, Pudong New District, Shanghai 200126, China*⁷*Department of Physics, New York University, New York, New York 10003, USA*

(Received 15 February 2023; revised 4 August 2023; accepted 5 September 2023; published 21 September 2023)

We develop a scheme to prepare a macroscopic maximally entangled state between two atomic ensembles using adaptive quantum nondemolition (QND) measurements. The quantum state of the system is evolved using a sequence of QND measurements followed by adaptive unitaries such that the desired measurement outcome is obtained with asymptotically unit probability. This procedure is repeated in z - and x -spin bases alternately such that the state converges deterministically towards the maximally entangled state. Up to a local spin-basis rotation, the maximally entangled state has zero total spin angular momentum, i.e., it is a singlet state. Our protocol does not perform postselection and works beyond the Holstein-Primakoff regime for the atomic spin degrees of freedom, producing genuine macroscopic entanglement.

DOI: [10.1103/PhysRevA.108.032420](https://doi.org/10.1103/PhysRevA.108.032420)**I. INTRODUCTION**

Entanglement plays an important role in various quantum information tasks such as teleportation [1], cryptography [2] and its production is one of the essential capabilities when constructing a quantum computer [3–5]. Entanglement is considered a resource in the context of quantum information science [6–10]. In the standard model of quantum computing, composite systems of qubits can be used to form a quantum register [4,11]. However, quantum protocols based on higher-dimensional systems have recently attracted a great attention [12–16] and offer certain advantages such as a higher information capacity and increased resistance to noise [17–20]. Higher-dimensional systems are advantageous as these allow for lower detection efficiency than qubits [21,22]. Several physical systems allow for the encoding of higher-dimensional quantum information. These systems include Rydberg atoms [23], trapped ions [24], cold atomic ensembles [25], superconducting phase qudits [26], photonic systems [27,28], and mechanical resonators [29]. Atomic gases are a particularly fascinating physical platform for observing many-body entanglement due to the high level of controllability and low decoherence [30,31]. One of the most elementary type of entangled states for an atomic gas is spin squeezed states, where particular observables are reduced below the standard quantum limit [32–34], and has numerous applications in quantum metrology [35–42]. It has also been observed that

Bell violations [43–45], which are a stronger form of quantum correlations in the quantum quantifier hierarchy [46,47], can be generated in Bose-Einstein condensates (BECs) [48,49].

Maximally entangled states such as Bell states in a two-qubit system [11,43,50,51] are of great importance for numerous quantum information tasks. Quantum communication schemes such as teleportation, dense coding, and entanglement swapping require control over a basis of maximally entangled quantum states [1,52,53]. In optical systems these states are routinely generated and detected [54]. In higher dimensions, maximally entangled states can potentially be used for the teleportation of more complex quantum states in the larger Hilbert space [55–58]. While most of the work relating to entanglement in atomic ensembles has been focused on the entanglement that exists between atoms in a single ensemble [35], works extending this to two or more spatially separate ensembles have also been investigated both theoretically and experimentally [30,59–62]. The first experimental demonstration of entanglement between atomic gases was observed in paraffin-coated hot gas cells [63] using quantum nondemolition (QND) measurements where the entanglement between two atomic ensembles had been produced in the form of two-mode squeezed states. For BECs, entanglement has been observed between two spatial regions of a single BEC [64–66]. Recently, entanglement between two separate BECs was also reported [67]. Such entanglement is fundamental to performing various quantum information tasks based on atomic ensembles, such as quantum teleportation [68–71], remote state preparation [72], clock synchronization [73], and quantum computing [74–76]. In the past, numerous theoretical and experimental works have been focused on generating

*manish.manish11167@gmail.com, manish.phys123@gmail.com

†tim.byrnes@nyu.edu

macroscopic singlet states within single atomic ensembles using collective QND measurement [77–79]. This state is basis invariant that finds considerable importance in quantum information processing [1,52,53,80,81]. Currently, the amount of entanglement that can be experimentally generated is very small, working within the Holstein-Primakoff approximation of spins, such that Hilbert space of the spins is largely unused. As such, current experiments are far below levels where a macroscopic maximally entangled state (MMES) can be generated even in principle from the way the protocols are constructed.

In this paper we propose a scheme for the generation of a MMES between two atomic ensembles using collective QND measurement and local spin rotations. In the QND scheme, the atoms in ensemble interact with a photonic field, which is subsequently measured, projecting the atoms into an entangled state [82,83]. Our approach extends works which have proposed sequential QND measurements to generate a collective singlet state within single atomic ensembles with postselection methods, such as in Refs. [77,79] and using feedback techniques [78]. Our scheme, on the other hand, is deterministic in the sense that the system converges towards a MMES with *asymptotically unit* probability as opposed to the stochastic evolution based on the random measurement outcomes in the sequential QND [83]. Our scheme does not approximate spins as a bosonic mode under the Holstein-Primakoff approximation as is often done by restricting to the short time interaction regime and holds for longer evolution times. In addition, our scheme does not rely upon individual atom control because we employ collective spin operations, projective measurements, and local unitary rotations that can be implemented in experimental settings.

The paper is structured as follows: In Sec. II we review the theory of QND measurement induced entanglement [82,83] and introduce the basic physical system that we are dealing with. In Sec. III we describe the maximally entangled state for macroscopic atomic ensembles and show its connection to the macroscopic singlet state. The former can be transformed into the latter state through a local unitary transformation. In Sec. IV we explain the protocol for deterministic preparation of the MMES and show that multiple sequential QND measurement produces a convergence of the desired state with the adaptive unitary. In Sec. V we numerically simulate our proposed protocol and show that convergence is obtained towards the MMES. In Sec. VI, we have discussed the overall effectiveness of the protocol with imperfections such as atom number fluctuations and initial ensemble prepared in the maximally mixed state. In Sec. VII, we propose an experimental setup to realize the protocol. Finally, in Sec. VIII we summarize our results.

II. QUANTUM NONDEMOLITION MEASUREMENTS

Here we review the theory of QND measurements on the atomic ensembles as introduced in Ref. [82]. The effect of multiple such QND entanglement operations is studied in Ref. [83].

A. Definitions and physical system

The physical system we shall consider consists of two neutral atomic ensembles or BECs, where each atom has two

populated internal states. A common choice for the internal states are hyperfine ground states, such as the $F = 1, m_F = -1$ and $F = 2, m_F = 1$ states in the case of ^{87}Rb [84]. For BECs we denote the bosonic annihilation operator for the two states as g_l, e_l , respectively, where $l \in \{1, 2\}$ labels the two BECs. These operators can be used to define an effective spin using the Schwinger boson operators

$$\begin{aligned} S_l^x &= e_l^\dagger g_l + g_l^\dagger e_l, \\ S_l^y &= -ie_l^\dagger g_l + ig_l^\dagger e_l, \\ S_l^z &= e_l^\dagger e_l - g_l^\dagger g_l. \end{aligned} \quad (1)$$

The commutation relation for the spin operators are

$$[S^j, S^k] = 2i\epsilon_{jkl}S^l, \quad (2)$$

where ϵ_{jkl} is the Levi-Civita symbol.

For atomic ensembles, the total spin operators are written in terms of collective spin operators:

$$\begin{aligned} S_l^x &= \sum_{n=1}^N \sigma_{l,n}^x, \\ S_l^y &= \sum_{n=1}^N \sigma_{l,n}^y, \\ S_l^z &= \sum_{n=1}^N \sigma_{l,n}^z, \end{aligned} \quad (3)$$

where $\sigma_{l,n}^k$ is a Pauli operator for the n th atom in the l th ensemble. For simplicity, we consider that each ensemble has the same number N of atoms. For the case that all the operations on the atomic ensembles are completely symmetric under particle interchange from the initialization of the states to the final measurement, the formalism (1) and (3) for the BECs and atomic ensembles, respectively, are completely equivalent [85]. We use the bosonic formulation (1) henceforth, although it should be understood that our calculations apply to both the BEC and atomic ensemble cases.

The spin coherent states for N uncorrelated atoms in an ensemble is defined as

$$|\theta, \phi\rangle_l = \frac{(\cos \frac{\theta}{2} e^{-i\phi/2} e_l^\dagger + \sin \frac{\theta}{2} e^{i\phi/2} g_l^\dagger)^N}{\sqrt{N!}} |\text{vac}\rangle, \quad (4)$$

where θ, ϕ are the angles on the Bloch sphere and $|\text{vac}\rangle$ is the vacuum state containing no atoms. The Fock states are defined as

$$|k\rangle_l = \frac{(e_l^\dagger)^k (g_l^\dagger)^{N-k}}{\sqrt{k!(N-k)!}} |\text{vac}\rangle. \quad (5)$$

The Fock states are eigenstates of the S^z operator according to

$$S_l^z |k\rangle_l = (2k - N) |k\rangle_l. \quad (6)$$

B. Quantum nondemolition entanglement

Here we summarize the elementary entangling operation that we use in our protocol for deterministic preparation of maximally entangled states. Coherent light is used to perform an indirect measurement of two atomic ensembles arranged in a Mach-Zehnder configuration (Fig. 1). The atoms in the

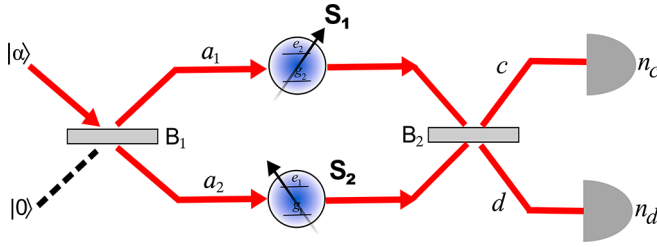


FIG. 1. Entanglement generation between two atomic ensembles using the QND scheme. Coherent light $|\alpha\rangle$ is used to interact two-mode BECs via the QND Hamiltonian interaction (7) arranged in a Mach-Zehnder configuration. The photon mode detections n_c, n_d after the second beam splitter B_2 entangles the two spins S_1 and S_2 .

ensemble are prepared in a product state of two spin coherent states and the interaction between photons and atoms is governed by the Hamiltonian [34]

$$H = \kappa (S_1^z - S_2^z) J^z, \quad (7)$$

where κ is the coupling constant and $J^z = a_1^\dagger a_1 - a_2^\dagger a_2$ is the Stokes operator for the two optical modes a_1, a_2 that enter into each arm of the interferometer.

After interacting with the atoms, the photonic modes are interfered with a beam splitter, giving rise to new modes c, d and the photons are detected by the detectors with counts n_c, n_d , respectively. After the measurement, the atomic ensembles collapse in the $S_1^z - S_2^z$ spin observable basis [82,83].

As shown in Ref. [83], the QND entanglement scheme between two atomic ensembles can be described in terms of a positive operator valued measure (POVM) as

$$M_{n_c n_d}(\tau) = \sum_{k_1, k_2=0} C_{n_c, n_d}[(k_1 - k_2)\tau] |k_1, k_2\rangle \langle k_1, k_2|, \quad (8)$$

where the modulating function is defined as

$$C_{n_c, n_d}(\chi) = \frac{\alpha^{n_c + n_d} e^{-|\alpha|^2/2}}{\sqrt{n_c! n_d!}} \cos^{n_c}(\chi) \sin^{n_d}(\chi), \quad (9)$$

and $\tau = \kappa t$ is the interaction time. The resulting state after the measurement is

$$\begin{aligned} |\tilde{\psi}_{n_c n_d}(\tau)\rangle &= M_{n_c n_d}(\tau) |\psi_0\rangle \\ &= \sum_{k_1, k_2} \langle k_1, k_2 | \psi_0 \rangle C_{n_c, n_d}[(k_1 - k_2)\tau] |k_1, k_2\rangle. \end{aligned} \quad (10)$$

According to Eq. (10), the initial wave function is modulated by an extra factor of $C_{n_c, n_d}[(k_1 - k_2)\tau]$ which can result in a measurement-induced generation of entanglement.

For large photon counts, the modulating function $C_{n_c, n_d}[(k_1 - k_2)\tau]$ takes a Gaussian form [82] and is sharply peaked at

$$\sin^2[(k_1 - k_2)\tau] = \frac{n_d}{n_c + n_d}. \quad (11)$$

Taking the interaction time $\tau = \pi/2N$ and assuming $|\alpha\tau|^2 \gg 1$, as defined in Ref. [83], we may then approximate the POVM (8) as a measurement operator according to

$$M_{n_c n_d} \left(\tau = \frac{\pi}{2N} \right) \approx \Pi_\Delta, \quad (12)$$

where the projections $\Delta = k_1 - k_2$ and photonic measurements n_c, n_d are related according to (11), and we defined

$$\begin{aligned} \Pi_\Delta &= \frac{1}{2^{\delta_\Delta}} \left(\sum_{k=0}^{N-\Delta} |k, k + \Delta\rangle \langle k, k + \Delta| \right. \\ &\quad \left. + (-1)^{(1-\delta_\Delta)n_d} \sum_{k'=\Delta}^N |k', k' - \Delta\rangle \langle k', k' - \Delta| \right). \end{aligned} \quad (13)$$

Here δ_Δ is the Kronecker delta which is one if $\Delta = 0$ and zero otherwise.

As it is clear from the definition of modulating function (9) and noted in Ref. [83], there is a sign difference between the two terms for odd n_d photonic measurements. Since the shot-to-shot photonic outcome n_d is random, the two measurements (13) occur randomly and leads to stochastic evolution of the system. An exception is the outcome $\Delta = 0$ which is independent of photonic count n_d . We show that, in our protocol, it is possible to construct an adaptive unitary that is independent of n_d (and thus avoids explicit photon counting) and still converges towards the MMES.

The measurement operators are defined in different spin bases by applying suitable unitary rotation as [85]

$$\Pi_\Delta^{(\theta, \phi)} = \mathcal{U}(\theta, \phi) \Pi_\Delta^{(z)} \mathcal{U}^\dagger(\theta, \phi), \quad (14)$$

where

$$\mathcal{U}(\theta, \phi) = e^{-i(S_1^z + S_2^z)\phi/2} e^{-i(S_1^y + S_2^y)\theta/2}, \quad (15)$$

and $\Pi_\Delta^{(z)}$ is the same measurement operator as in (13), but we explicitly specified the basis with the (z) label.

III. THE MAXIMALLY ENTANGLED STATE

In this section we discuss the nature of the maximally entangled state between two BECs. Namely, we would like to create the state

$$|\text{MMES}\rangle = \frac{1}{\sqrt{N+1}} \sum_k |k\rangle_1 |k\rangle_2. \quad (16)$$

This state has an entanglement of $E = \log_2(N+1)$ using the von Neumann entropy, which is the maximum value for two $(N+1)$ -level systems. This state is also known as the spin-EPR state for atomic ensembles [86].

We now show that the MMES (16) has a very close connection with the spin-zero singlet state. This fact shall be used to construct our protocol. Each BEC can be considered to be a macroscopic qubit state with spin value $s_1 = s_2 = N/2$. Due to each boson being symmetric under interchange, the total spin is always in the maximum spin sector. For two spins, one can define the collective state that can be formed, with quantum numbers of the total spin $s_{\text{tot}} = s_1 + s_2$, here we have used the notation $s_l = S_l/2$, to connect our notation to the standard conventions of quantum angular momentum and $l \in \{1, 2\}$ labels two atomic ensembles. We can explicitly write this state in terms of the total angular momentum eigenstate $|s, m\rangle$ where the two spins are coupled with $m = m_1 + m_2$, m is the orientation of total spin quantum number s along the z

direction such that

$$\begin{aligned} (s_1^z + s_2^z)|s, m\rangle &= m|s, m\rangle, \\ s_{\text{tot}}^2|s, m\rangle &= s(s+1)|s, m\rangle. \end{aligned} \quad (17)$$

There is a unique singlet state $|s_0, m_0\rangle$ which satisfies

$$\begin{aligned} (s_1^z + s_2^z)|s_0, m_0\rangle &= 0, \\ s_{\text{tot}}^2|s_0, m_0\rangle &= 0, \end{aligned} \quad (18)$$

with $s_0 = m_0 = 0$. Using the coupling rule for two spins [87], the singlet state then reads

$$|s_0, m_0\rangle = \sum_m \frac{(-1)^{s-m}}{\sqrt{2s+1}} |s, m\rangle_1 |s, -m\rangle_2. \quad (19)$$

The state (19) has perfect correlations and anticorrelations in the linear combination of spin observables. The state could be realized as the ground spin state of the Hamiltonian S^2 .

For atomic ensembles of collection of N atoms, we describe the state in Fock space (5) that can be equivalently described in the angular momentum basis as well

$$|k\rangle = \left| s = \frac{N}{2}, m = k - \frac{N}{2} \right\rangle. \quad (20)$$

The singlet state (19) is defined for atomic ensemble using the relation (20):

$$|s_0, m_0\rangle = \frac{1}{\sqrt{N+1}} \sum_{k=0}^N (-1)^k |k\rangle_1 |N-k\rangle_2. \quad (21)$$

We see that there is a close connection between the maximally entangled state (16) and the singlet state (21). In fact, the singlet state is a MMES up to a local basis transformations. The local spin basis rotation,

$$e^{-iS_2^y \frac{\pi}{2}} |k\rangle = (-1)^k |N-k\rangle, \quad (22)$$

transforms the singlet state to the maximally entangled state as

$$|\text{MMES}\rangle = e^{-iS_2^y \frac{\pi}{2}} |s_0, m_0\rangle. \quad (23)$$

From (23) we may deduce the operator that has the analogous relation as (18) for the MMES. Applying the operator $e^{-iS_2^y \pi/2}$ to (18) and using (23) we have

$$e^{-iS_2^y \pi/2} s_{\text{tot}}^2 e^{iS_2^y \pi/2} |\text{MMES}\rangle = \bar{s}_{\text{tot}}^2 |\text{MMES}\rangle = 0, \quad (24)$$

where

$$\bar{s}_{\text{tot}}^2 = \frac{(S_1^x - S_2^x)^2 + (S_1^y + S_2^y)^2 + (S_1^z - S_2^z)^2}{4} \quad (25)$$

has same correlations in the spin observables as seen in QND interactions [82,83].

For a two-qubit system, the maximally entangled state (16) is the Bell state

$$\frac{|0\rangle_1 |0\rangle_2 + |1\rangle_1 |1\rangle_2}{\sqrt{2}}. \quad (26)$$

This state is an eigenstate of the operators $\sigma_1^z - \sigma_2^z$ and $\sigma_1^x - \sigma_2^x$ with zero eigenvalue.

IV. DETERMINISTIC PREPARATION OF MAXIMALLY ENTANGLED STATE

As discussed in Sec. II, QND measurements can be used to entangle two different atomic ensembles or BECs. Depending on the photonic measurement outcomes, the state of BEC collapses on different entangled states in general (10). For instance, an initial state $|\psi_0\rangle$ is collapsed by measurement (13) as

$$\Pi_{\Delta}^{(z)} |\psi_0\rangle = \sum_{k=0}^{N-\Delta} \psi_k^+ |k+\Delta\rangle |k\rangle + \sum_{k'=\Delta}^N \psi_{k'}^- |k'-\Delta\rangle |k'\rangle, \quad (27)$$

where the coefficients in (27)

$$\begin{aligned} \psi_k^+ &= \frac{1}{2^{\delta_{\Delta}}} \langle k+\Delta | \langle k | \psi_0 \rangle, \\ \psi_k^- &= \frac{(-1)^{(1-\delta_{\Delta})m_d}}{2^{\delta_{\Delta}}} \langle k-\Delta | \langle k | \psi_0 \rangle, \end{aligned} \quad (28)$$

which is an entangled state for a particular measurement outcome Δ . It is, however, not a MMES due to the amplitudes ψ_k^{\pm} being not necessarily of equal magnitude, and the difference Δ between the Fock states in the BECs. Our aim now will be to devise a protocol such that the MMES (16) can be prepared deterministically using quantum measurements which are inherently random.

A. Basic idea

To gain some intuition about the protocol that we introduce later, let us introduce some basic properties of the QND measurements and the MMES.

The MMES is a unique state that is an eigenstate of both the measurement operators $\Pi_0^{(z)}$ and $\Pi_0^{(x)}$,

$$\begin{aligned} \Pi_0^{(z)} |\text{MMES}\rangle &= |\text{MMES}\rangle, \\ \Pi_0^{(x)} |\text{MMES}\rangle &= |\text{MMES}\rangle. \end{aligned} \quad (29)$$

It then follows that an alternating sequence of such measurements has the $|\text{MMES}\rangle$ as an eigenstate

$$(\Pi_0^{(x)} \Pi_0^{(z)})^M |\text{MMES}\rangle = |\text{MMES}\rangle. \quad (30)$$

Due to the unique nature of the MMES satisfying (29), the QND measurements (13) applied alternately on an arbitrary state $|\psi_0\rangle$ converges to the MMES (16),

$$(\Pi_0^{(x)} \Pi_0^{(z)})^M |\psi_0\rangle \xrightarrow{M \rightarrow \infty} |\text{MMES}\rangle. \quad (31)$$

According to (29), since the MMES is an eigenstate of both $\Pi_0^{(z)}$ and $\Pi_0^{(x)}$ measurement operators, once the state $|\text{MMES}\rangle$ is obtained, further application of the measurement operators do not change the state. This is in fact a unique state for the same reasons that a singlet state is a unique state for two $s_l = N/2$ spins. Therefore it is a fixed point of the evolution. The MMES is obtained for the QND measurement (13) corresponding to outcome $\Delta = 0$. However, Eq. (31) does not constitute a physically realizable protocol because obtaining the $\Delta = 0$ measurement outcome is set by Born's probability rule and due to the randomness of quantum measurements, we cannot guarantee that only the $\Delta = 0$ outcome will be obtained.

To overcome the randomness of quantum measurements and make a deterministic scheme, we use an adaptive strategy. Our scheme involves applying a unitary transformation to the state in the event that a $\Delta \neq 0$ is obtained, and repeating the measurements many times until the desired $\Delta = 0$ outcome is obtained. The protocol is deterministic in the sense that eventually a measurement sequence will always end up with the $\Delta = 0$ outcome. The adaptive unitary is chosen such as to maximize the probability of obtaining the $\Delta = 0$ outcome in the next step. Our approach can be considered a special case of the measurement-based imaginary time evolution protocol proposed in Refs. [88,89].

B. Protocol

Here we more concretely describe the full procedure for deterministic preparation of the MMES using sequential QND measurements performed in z and x basis. We define the “repeat-until-success” adaptive QND scheme which applies a sequence of QND measurements (13) and unitary operators until the measurement outcome $\Delta = 0$ is obtained as

$$\begin{aligned} T_{\Delta}^{(z)} &= \prod_{j=1}^L U_{\Delta_j}^{(z)} \Pi_{\Delta_j}^{(z)} \\ &= \Pi_0^{(z)} U_{\Delta_{L-1}}^{(z)} \Pi_{\Delta_{L-1}}^{(z)} \dots U_{\Delta_1}^{(z)} \Pi_{\Delta_1}^{(z)}, \end{aligned} \quad (32)$$

where $\Delta_L = 0$ and $U_0^{(z)} = I$. A particular repeat-until-success measurement sequence is labeled according to the notation

$$\vec{\Delta} = (\Delta_1, \Delta_2, \dots, \Delta_L). \quad (33)$$

To make the state convergent towards MMES, we aim to correct those projections ($\Delta \neq 0$) through unitary $U_{\Delta}^{(z)}$ that ensures the convergence,

$$\Pi_0^{(z)} |\tilde{\psi}_{\vec{\Delta}}\rangle = |\tilde{\psi}_{\vec{\Delta}}\rangle, \quad (34)$$

where the unnormalized state after the repeat-until-success sequence is

$$|\tilde{\psi}_{\vec{\Delta}}\rangle = T_{\vec{\Delta}}^{(z)} |\psi_0\rangle. \quad (35)$$

Then analogously to (31), we replace each of the projectors in the z and x basis with the measurement sequences (32) such that

$$|\tilde{\psi}_{\vec{\Delta}}^f\rangle = \prod_{r=1}^M (T_{\vec{\Delta}_r^x}^{(x)} T_{\vec{\Delta}_r^z}^{(z)}) |\psi_0\rangle \xrightarrow{M \rightarrow \infty} |\text{MMES}\rangle, \quad (36)$$

where the product is evaluated in the reverse order such that $r = 1$ is applied first. The full sequence for the adaptive sequential QND measurements is written

$$\vec{\Delta} = (\vec{\Delta}_1^z, \vec{\Delta}_1^x, \vec{\Delta}_2^z, \vec{\Delta}_2^x, \dots, \vec{\Delta}_M^z, \vec{\Delta}_M^x). \quad (37)$$

The two repeat-until-success sequences in the z and x basis are repeated until convergence is attained and defined as obtaining the outcome $\Delta = 0$ for the first measurement in each repeat-until-success sequence.

Here we summarize, for the sake of clarity, the entire protocol for preparing the MMES using adaptive QND scheme (Fig. 2). The protocol follows the following sequence:

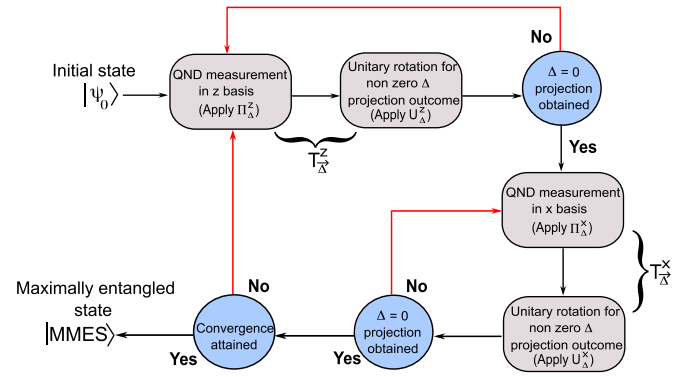


FIG. 2. Protocol for obtaining the MMES. A “repeat-until-success” measurement sequence $T_{\vec{\Delta}}^{(z)}$ is applied to an initial state, where a sequence of projective measurements $\Pi_{\Delta}^{(z)}$ and adaptive unitary rotations are made until the $\Delta = 0$ result is obtained. The same repeat-until-success sequence is repeated in the x basis. The two sequences are repeated until convergence is attained, where both z and x measurements yield $\Delta = 0$ on the first measurement. This procedure converges to the MMES (16).

(1) Perform the repeat-until-success $\Pi_{\Delta}^{(z)}$ QND measurement sequence in the z basis. If $\Delta \neq 0$, then apply unitary $U_{\Delta}^{(z)}$ as a correction and reapply $\Pi_{\Delta}^{(z)}$ until the measurement outcome $\Delta = 0$ is obtained (32).

(2) Do the same as step 1 in the x basis in order to converge towards $\Delta = 0$ measurement outcome.

(3) Repeat steps 1 and 2 until the outcome $\Delta = 0$ is obtained for both on the first measurement for a satisfactory number of cycles (36).

The above sequence, using adaptive QND, deterministically converges an initial state to a MMES (23).

C. The adaptive unitary

In this section we discuss the choice of unitary rotation that is employed in the repeat-until-success sequence. There is in fact no unique choice for the adaptive unitary and we take advantage of this to choose a convenient form that has a simple experimental implementation. To understand the different choice of the unitary rotation, we first analyze the state

$$|\tilde{\psi}_{\vec{\Delta}}^c\rangle = U_{\vec{\Delta}}^{(z)} \Pi_{\vec{\Delta}}^{(z)} |\psi_0\rangle. \quad (38)$$

The main criterion for the unitary correction is that it maximizes the probability that $\Delta = 0$ is obtained in the next outcome. As may be seen by the measurement operator (13), there are two outcomes which occur randomly depending on detection count of the photonic outcomes n_d . We assume that n_d is not measurable, since it requires single-photon resolution of a bright laser, which is experimentally challenging. To overcome this, we choose a unitary correction that rotates the state such that it has a significant overlap with the $\Delta = 0$ sector, regardless of the random outcome of n_d in QND measurements (13). In the previous works of Refs. [77,79], postselection based on the measurement outcomes was utilized to target singlet states with $\mathbf{S} = 0$. Additionally, a feedback mechanism [78] was employed to enhance the spin correlations with $\mathbf{S} = 0$. Our scheme shares similarities with these coherent

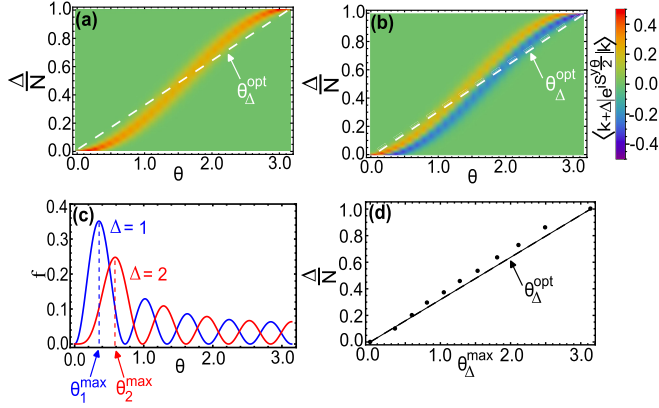


FIG. 3. Choice of optimum angle of unitary transformation: Plot of the matrix element $\langle k + \Delta | e^{iS^y \theta/2} | k \rangle$ given in (A1) as a function of the angle of unitary rotation θ in (39) with the measurement outcome Δ in (33) for (a) $k = 0$, (b) $k = 1$. Total number of the atoms is $N = 150$, (c) Variation of the fidelity (42) with the angle of unitary rotation (39) in the adaptive QND measurement outcomes, $N = 10$. $\theta_{\Delta}^{\text{max}}$ represents angle of unitary rotation that maximizes the fidelity (42) for a particular measurement outcome Δ . (d) Plot of maximized angles of unitary rotation for different measurement outcome (38), $N = 10$. The dashed line in panels (a), (b), and (d) depicts the optimized choice of unitary rotation that maximizes the fidelity, which is fit with the line $\theta_{\Delta}^{\text{opt}} = \pi \frac{\Delta}{N}$.

feedback techniques because it aims to create the spin correlations present in a MMES in subsequent rounds of QND measurements in a deterministic sense.

We choose a unitary transformation that is based on a spin rotation

$$U_{\Delta}^{(z)} = e^{iS_1^y \frac{\theta_{\Delta}}{2}} \otimes I_2. \quad (39)$$

We require a relationship between the measurement outcome Δ and the corresponding angle of rotation θ . An adaptive unitary (39) changes the QND measured initial state (27) as

$$\begin{aligned} U_{\Delta}^{(z)} \Pi_{\Delta}^{(z)} |\psi_0\rangle &= \sum_{k=0}^{N-\Delta} \sum_{k'=0}^N \psi_k^+ \langle k' | e^{iS_1^y \frac{\theta_{\Delta}}{2}} | k + \Delta \rangle | k' \rangle_1 | k \rangle_2 \\ &+ \sum_{k=\Delta}^N \sum_{k'=0}^N \psi_k^- \langle k' | e^{iS_1^y \frac{\theta_{\Delta}}{2}} | k - \Delta \rangle | k' \rangle_1 | k \rangle_2. \end{aligned} \quad (40)$$

We see that the modified state (40) involves the matrix elements of unitary rotations $e^{iS^y \theta/2}$.

To maximize the probability that the outcome $\Delta = 0$ in the next measurement is obtained, we require performing a rotation within the state space that transforms the random projected state to MMES while maintaining the overall coherence and entanglement properties. Mathematically, it translates to maximizing the amplitudes of the terms with $k' = k$ in (40), such that the matrix elements $\langle k | e^{iS^y \theta/2} | k \pm \Delta \rangle$ have a large value (see Appendix for an explicit expression of the matrix elements).

Figures 3(a) and 3(b) show the plot of the amplitude of matrix element $\langle k + \Delta | e^{iS^y \theta/2} | k \rangle$ for two values of $k = 0, 1$, respectively. We can see that the largest amplitudes occur for

a unitary rotation corresponding to a particular outcome Δ near to the curve

$$\theta_{\Delta} \propto \frac{\Delta}{N}. \quad (41)$$

We see that, as k increases in Figs. 3(a) and 3(b), the region where the matrix elements have a significant magnitude broadens.

To find the proportionality constant in (41), we analyze the overlap of the transformed state with MMES. The fidelity of the normalized state (38) with the MMES (16) is calculated after the first QND measurement as

$$f = \frac{|\langle \text{MMES} | \tilde{\psi}_{\Delta}^c \rangle|^2}{\langle \tilde{\psi}_{\Delta}^c | \tilde{\psi}_{\Delta}^c \rangle}. \quad (42)$$

Figure 3(c) shows the variation of the fidelity of the state when the angle of unitary rotation is varied. We can see that the fidelity is maximum for a particular angle of unitary rotation $\theta_{\Delta}^{\text{max}}$. It is clear that the choice of the angle is unique that maximizes the fidelity.

Figure 3(d) shows the possible choice for the angle of unitary rotation, we see that the largest amplitude occurs near to the line

$$\theta_{\Delta}^{\text{opt}} = \pi \frac{\Delta}{N}. \quad (43)$$

This corrects the state (38) in such a way that it has a large overlap with the MMES (16) in the next round of measurement. We note that it is possible to further improve upon the choice (43), but we find that this is a simple but effective choice that works for all N .

V. PERFORMANCE OF THE ADAPTIVE QUANTUM NONDEMOLITION SCHEME

To demonstrate that the MMES is prepared using our protocol, we have performed a numerical analysis to check the effectiveness of the protocol.

A. Convergence to desired measurements

We first examine the probability distribution of the state after one QND measurement and correction step (35) in the z basis according to the protocol. The probability of a particular sequence is defined by,

$$\begin{aligned} p_{\bar{\Delta}} &= \langle \tilde{\psi}_{\bar{\Delta}} | \tilde{\psi}_{\bar{\Delta}} \rangle \\ &= \langle \psi_0 | T_{\bar{\Delta}}^{(z)\dagger} T_{\bar{\Delta}}^{(z)} | \psi_0 \rangle, \end{aligned} \quad (44)$$

where the normalized state (35) of the protocol is given by

$$|\psi_{\bar{\Delta}}\rangle = \frac{|\tilde{\psi}_{\bar{\Delta}}\rangle}{\sqrt{\langle \tilde{\psi}_{\bar{\Delta}} | \tilde{\psi}_{\bar{\Delta}} \rangle}}. \quad (45)$$

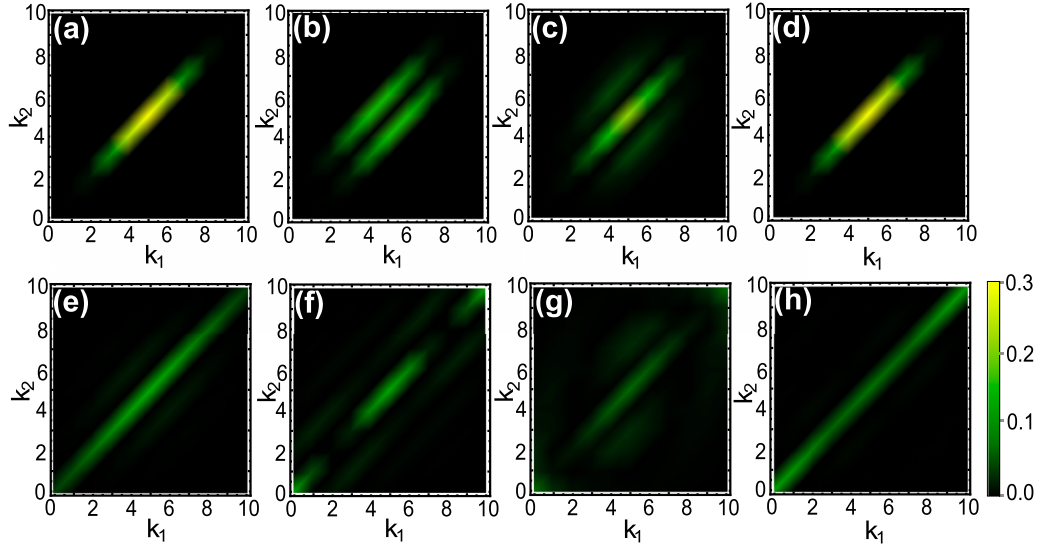


FIG. 4. Plots for the probability distribution (48) of the initial state (46) after sequential adaptive QND measurement (36) in the z and subsequently in the x basis for operators (a) Π_0^z , (b) Π_1^z , (c) $U_1^x \Pi_1^z$, (d) $\Pi_0^z U_1^x \Pi_1^z$, (e) $\Pi_0^x \Pi_0^z$, (f) $\Pi_2^x \Pi_0^z$, (g) $U_2^x \Pi_2^x \Pi_0^z$, and (h) $\Pi_0^x U_2^x \Pi_2^x \Pi_0^z$. The number of atoms in each ensemble is $N = 10$.

We consider the initial state of the two atomic ensembles to be an S^x -polarized state,

$$\begin{aligned} |\psi_0\rangle &= \left| \frac{\pi}{2}, 0 \right\rangle_1 \left| \frac{\pi}{2}, 0 \right\rangle_2 \\ &= \frac{1}{2^N} \sum_{k_1, k_2=0}^N \sqrt{\binom{N}{k_1} \binom{N}{k_2}} |k_1, k_2\rangle. \end{aligned} \quad (46)$$

The operator $T_{\Delta}^{(z)}$ applied on the initial state (46) produces correlations between the BECs in the z basis. In the case of obtaining $\Delta = 0$ outcome on the first measurement, the state that is obtained is

$$\begin{aligned} \Pi_{\Delta}^z |\psi_0\rangle &= \frac{1}{2^N} \sum_{k=0}^N \binom{N}{k} |k, k\rangle \\ &= \sum_{k=0}^N \sqrt{p_0(k, k)} |k, k\rangle, \end{aligned} \quad (47)$$

where $p_{\Delta}(k_1, k_2) = |\langle k_1, k_2 | \Pi_{\Delta}^z |\psi_0\rangle|^2$ is the probability of the measured state for a particular outcome Δ in the Fock basis. The outcome $\Delta = 0$ signifies the MMES-like correlations (16).

In general, for a random measurement sequence (36), the probability distribution in the Fock states is described as

$$p_{\Delta}^z(k_1, k_2) = |\langle k_1, k_2 | T_{\Delta}^{(x)} T_{\Delta}^{(z)} |\psi_0\rangle|^2. \quad (48)$$

In Fig. 4 we plot the probability distribution of the state (48) after performing a QND measurement and correction operations in the z and x bases, respectively. In Figs. 4(a)–4(d) we show the probability distributions for one measurement and unitary correction sequence in the z basis. In Fig. 4(a) we see that the probability distribution for $\Delta^z = 0$ is correlated along $k_1 = k_2$ in the Fock state space of two ensembles and it

resembles that of the MMES distribution (16). It is, however, not the MMES because of the binomial factors in (47). For the projection outcomes $\Delta^z = 1$ in Fig. 4(b), we see the offset in Fock state probability distribution with $k_2 = k_1 \pm \Delta^z$ according to the definition of operator (13). By applying a unitary correction (39), mostly the probability distribution is restored along the diagonal, as shown in Fig. 4(c), such that in the subsequent measurement there is a high probability of obtaining $\Delta^z = 0$ in Fig. 4(d).

Figures 4(e)–4(h) show the effect of another application of the sequence of QND measurements (32), where the basis is changed from z to x . Correlations are further improved in Fig. 4(e) because of suppression of the binomial factors (47). Unlike Fig. 4(b), we observe weaker offsets in the Fock state space as it is clear from Figs. 4(g)–4(h). It is because of the fact that in subsequent QND measurement and corrections, stronger spin correlations are developed only for the MMES. Hence, the probability of obtaining the prepared state in other measurement outcomes, such as $\Delta^x \neq 0$, is less likely and the probability distribution converges solely towards that of the MMES in Fig. 4(f) which implies the deterministic preparation of an initial state from the scheme.

B. Probability distribution

We now turn to the probability (44) of the various measurement outcomes in the protocol, shown in Fig. 5. We define the marginal probability distribution of obtaining the measurement outcomes in a particular sequence (33) as

$$p_{\Delta_L} = \sum_{\Delta_1, \Delta_2, \dots, \Delta_{L-1}} p_{\bar{\Delta}}. \quad (49)$$

The marginal probability gives the total probability of obtaining an outcome Δ_L in a sequence of L measurements (33). This gives the probability of obtaining an outcome Δ_L in a sequence, regardless of the previous measurement outcomes.

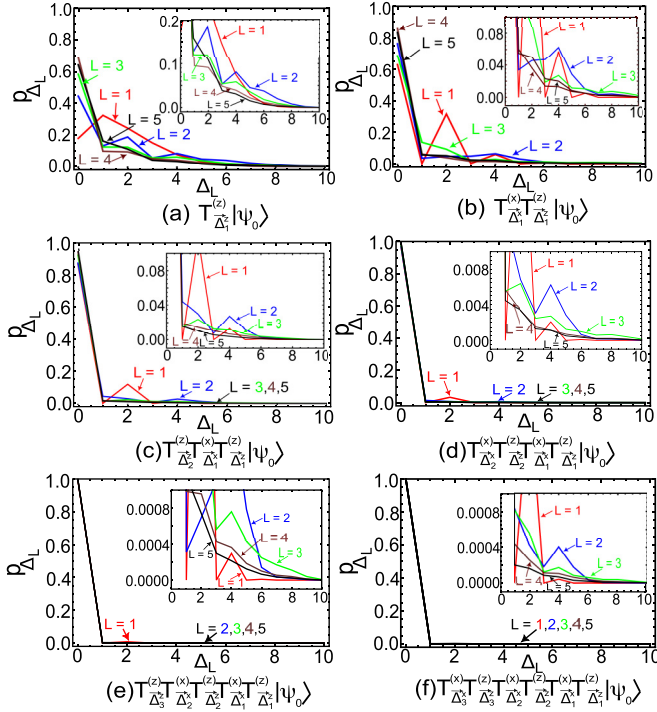


FIG. 5. Marginal probability (49) for different measurement outcomes in sequential adaptive QND measurement (36) is shown for two atomic ensembles prepared in S^x -polarized state (46). Convergence is attained for measurement outcome $\Delta = 0$ after three rounds of iterations. A zoomed in plot is shown in the inset for better visibility of the probability values and its convergence in a sequence. The number of atoms in each ensemble is $N = 10$.

In Fig. 5 we have plotted the marginal probabilities for various levels of iteration for different measurement sequences (32). Figure 5(a) shows a single z -basis measurement sequence. As we can see, the marginal probability for the initial state is generally largest for the outcome $\Delta = 0$ and the probability decreases for other outcomes $\Delta \neq 0$. The probability to obtain the MMES increases with larger numbers of measurements ($L = 5$) in a sequence. Figure 5(b) shows an x -basis sequence after an initial measurement sequence in the z basis, where the final outcome was $\Delta^z = 0$. The probability for obtaining the MMES increases successively with the measurement sequences as compared with Fig. 5(a) and hence, other probabilities corresponding to the measurement outcomes $\Delta \neq 0$ are suppressed further. Similarly, Figs. 5(c) and 5(d) show other z - and x -basis measurement sequences respectively ($M = 2$) after the first z - and x -basis sequence ($M = 1$), in this case the state converges to the MMES at a faster rate. The state is prepared in the measurement outcome $\Delta = 0$ with almost unit probability and the other measurement outcomes $\Delta \neq 0$ occur with low probability. Finally, Figs. 5(e) and 5(f) best describes the overall performance of the protocol as the probability of obtaining the outcome $\Delta = 0$ is dominant in the subsequent QND measurements in the z and x bases, respectively ($M = 3$), and the MMES is prepared with nearly 100% success with very little contribution from the other measurements because of the increasing spin

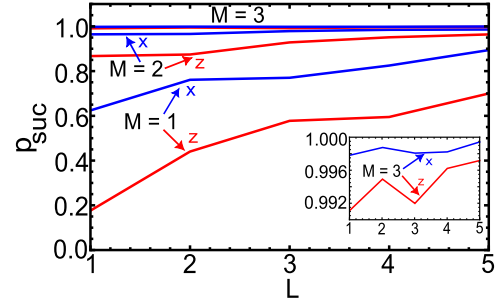


FIG. 6. Success probability (50) for obtaining the MMES after sequential adaptive QND measurement (36) for $M = 1, 2, 3$ is plotted. It shows the convergence to the desired state after each measurement in the z and x bases. A zoomed in plot is shown for $M = 3$ in the inset. The number of atoms in each ensemble is $N = 10$.

correlations. This shows that the MMES can be prepared in a deterministic way.

C. Success probability

In the previous section, we have seen that in the sequential adaptive QND measurements, the probability of obtaining $\Delta \neq 0$ measurement outcomes is low and the system is prepared deterministically in the MMES with outcome $\Delta = 0$. We define the success probability for obtaining the MMES as a sum of the probability of all the measured states in a QND measurement sequence with measurements that end with $\Delta = 0$:

$$\begin{aligned} p_{\text{suc}} &= p_{\Delta_L=0} \\ &= \sum_{\Delta_L \in \{0\}} \sum_{\Delta_1, \Delta_2, \dots, \Delta_{L-1}} p_{\bar{\Delta}}. \end{aligned} \quad (50)$$

Figure 6 shows the success probability of obtaining the MMES in our protocol for various levels of iteration. We see that after a single z -basis measurement sequence (e.g., the $M = 1$ case), the success probability increases monotonically, as expected, although it is not sufficient to drive towards a perfect MMES because other measurement outcomes are still possible [see also Fig. 5(a)]. Another measurement sequence in x basis leads to enhanced spin correlations and an increased probability for obtaining $\Delta = 0$ outcome, so it shows better success probability. Similarly in the next round of measurements in the z and x bases, i.e., $M = 2$, near unit success probability is achieved. After three rounds of measurements ($M = 3$), the success probability of obtaining the MMES is close to unity. The convergence to unit probability is shown in the inset for better clarity.

D. Fidelity calculation

Finally, we calculate the fidelity of the final state obtained from the protocol. The fidelity of the normalized state (36) with respect to the MMES in an adaptive QND measurement sequence (37) is calculated as

$$F_{\bar{\Delta}} = \frac{|\langle \text{MMES} | \tilde{\psi}_{\bar{\Delta}}^f \rangle|^2}{\langle \tilde{\psi}_{\bar{\Delta}}^f | \tilde{\psi}_{\bar{\Delta}}^f \rangle}. \quad (51)$$

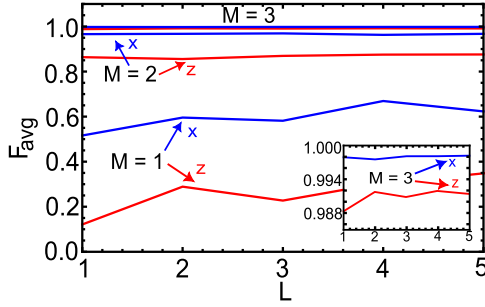


FIG. 7. Average fidelity (52) of the initial state (46) for different measurement outcomes is calculated in adaptive QND measurement (36) for $M = 1, 2, 3$. Convergence is attained after three rounds of measurements. A zoomed-in plot is shown for $M = 3$ in the inset. The number of atoms in each ensemble is $N = 10$.

We also define the fidelity over all possible outcomes, the average fidelity is calculated as

$$F_{\text{avg}} = \sum_{\bar{\Delta}} p_{\bar{\Delta}} F_{\bar{\Delta}} = |\langle \text{MMES} | \prod_{r=1}^M (T_{\bar{\Delta}_r^x}^{(x)} T_{\bar{\Delta}_r^z}^{(z)}) | \psi_0 \rangle|^2, \quad (52)$$

where the probability of a state in a particular sequence is

$$p_{\bar{\Delta}} = \langle \tilde{\psi}_{\bar{\Delta}}^f | \tilde{\psi}_{\bar{\Delta}}^f \rangle. \quad (53)$$

Figure 7 shows the average fidelity for obtaining the MMES for our protocol (36). In the first z -basis measurement, the average fidelity is low and it increases with the number of measurements made in a sequence. An x -basis measurement after an initial measurement sequence in the z basis in the final outcome $\Delta^z = 0$ improves the average fidelity as the probability for obtaining the MMES increases. In the next round of measurements in the z and x basis, i.e., $M = 2, 3$, the average fidelity increases to unity implying perfect preparation of the MMES only.

VI. EFFECT OF IMPERFECTIONS

Here we discuss the performance of the protocol with the possible sources of decoherence included. Specifically, we discuss the effect of the atom number fluctuations and the initial ensembles prepared in a maximally mixed state.

A. Initial maximally mixed state

We consider the initial state of the system to be a maximally mixed state described by

$$\rho_0 = \frac{I_1 \otimes I_2}{(N+1)^2}, \quad (54)$$

where I_j is the identity matrix in the Hilbert space for the j th ensemble. The procedure is identical to the pure state calculation performed earlier using the equations (50)–(52). The action of the first QND measurement in z -spin basis (32) transforms the density matrix, such that the protocol leads to

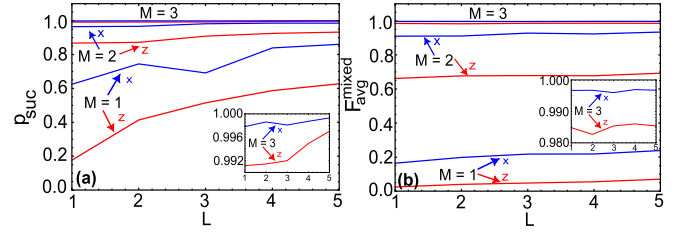


FIG. 8. The success probability (50) and average fidelity (52) of the initial mixed state (54) for obtaining the MMES after sequential adaptive QND measurement (36) for $M = 1, 2, 3$ is plotted. A zoomed in plot is shown for $M = 3$ in the inset. The number of atoms in each ensemble is $N = 10$.

the convergence to the MMES state,

$$\rho_{\bar{\Delta}} = \prod_{r=1}^M (T_{\bar{\Delta}_r^x}^{(x)} T_{\bar{\Delta}_r^z}^{(z)}) \rho_0 (T_{\bar{\Delta}_r^x}^{(x)} T_{\bar{\Delta}_r^z}^{(z)})^\dagger. \quad (55)$$

The fidelity is calculated as

$$F_{\bar{\Delta}}^{\text{mixed}} = \frac{\langle \text{MMES} | \rho_{\bar{\Delta}} | \text{MMES} \rangle}{\text{Tr}(\rho_{\bar{\Delta}})}, \quad (56)$$

and the average fidelity is expressed as

$$F_{\text{avg}}^{\text{mixed}} = \sum_{\bar{\Delta}} p_{\bar{\Delta}} F_{\bar{\Delta}}^{\text{mixed}}, \quad (57)$$

where the probability of a particular sequence is

$$p_{\bar{\Delta}} = \text{Tr}(\rho_{\bar{\Delta}}). \quad (58)$$

Figures 8(a) and 8(b) show the success probability and average fidelity using the above procedure. In Fig. 8(a), the probability of achieving the MMES increases in a similar sequential manner to that observed in Fig. 6. However, in Fig. 8(b), the fidelity of the prepared state is initially lower compared with that of Fig. 7. This discrepancy is in contrast to the initial spin coherent states (46) that collapses to the state (47) in a single QND measurement. This does not happen with the initial state in (54) and the convergence rate to the MMES is slower in the initial rounds of adaptive QND measurements. After two rounds, $M = 2$, this converges to the MMES rapidly, as seen in Fig. 8(b). Since the initial maximally mixed state lacks coherence, and any coherence is entirely produced by the subsequent QND and unitary rotations, its evolution within the adaptive QND scheme towards the MMES shows the overall robustness of the protocol.

B. Atom number fluctuations

In a typical experimental setup, BECs are not prepared with fixed atom number. In this section, we discuss the effect of the atom number fluctuations when both BECs are prepared as the statistical distribution of different atom numbers N . Here we consider an initial state that is a mixed state of various atom numbers according to

$$\rho_0 = \sum_{N_1, N_2} p(N_1) p(N_2) |\psi_0\rangle_{N_1, N_2} \langle \psi_0|_{N_1, N_2}. \quad (59)$$

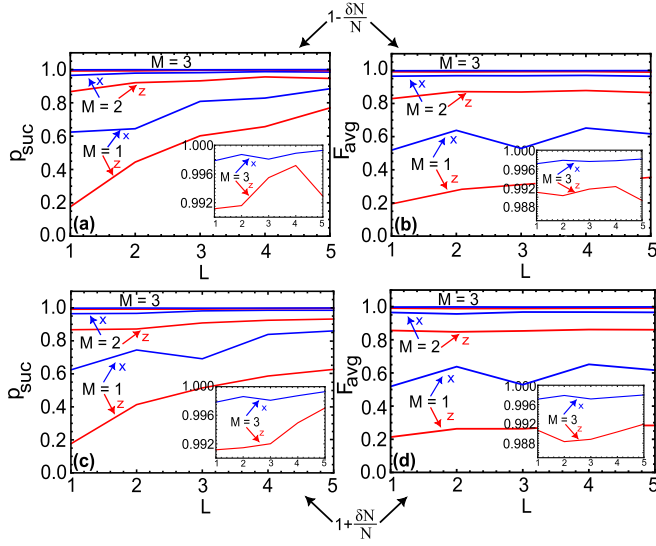


FIG. 9. Effect of the atom number fluctuations on the protocol: the success probability (50) and average fidelity (52) of the initial state (46) for obtaining the MMES after sequential adaptive QND measurement (36) for $M = 1, 2, 3$ is plotted. The corrective unitary rotation is applied considering the atom number variation in the range (60). The number of atoms in each ensemble is $N = 10$ and $\delta N/N = 14\%$.

Here, ρ_0 is the initial-state density matrix and the probabilities $p(N_j)$ are taken to be Gaussian distributions. When accounting for the fluctuations in the atom number for j th atomic ensemble, denoted $N_j \pm \delta N_j$, we observe different potential effects that could impact the performance of the protocol. First, the QND interaction and the adaptive unitary rotations themselves do not depend on the atom number N . All the operations are atom-number conserving. Hence the overall protocol is not modified with the change in N_j . For this reason, we have analyzed each particle number sector separately and calculate the fidelity for each sector with the initial state (46). The only thing that is sensitive is the angle of rotation, which involves the N_j dependence. With fluctuations in the atom number $N' = N \pm \delta N$, the unitary rotation angle is modified to

$$\theta_{\Delta}^{\text{opt}} \approx \theta_{\Delta}^{\text{opt}} \left(1 \pm \frac{\delta N}{N} \right). \quad (60)$$

In the recent experimental work of Ref. [90], it was found that $\delta N/N$ ranges between 10%–15%.

In Fig. 9 we have analyzed the effect of atom fluctuations on the protocol. Figures 9(a)–9(d) show the success probability and average fidelity for obtaining the MMES for various levels of iterations when $N' = N \pm \delta N$. Within a sequence, it follows a similar trend as observed with $\delta N = 0$ case in Figs. 6 and 7. Relative atom number fluctuations result in a random choice to the applied unitary corrections (60) and, hence, it leads to a nonmonotonic convergence to the MMES. Nevertheless the procedure converges to a MMES and it is clear that rotation with a suboptimal angle does not significantly affect the convergence of the protocol, implying the relative insensitivity of the atom number fluctuations on the scheme.

VII. EXPERIMENTAL IMPLEMENTATION

There are various physical systems that can be employed to implement the protocol and physical operations (Fig. 1) described in the previous sections. One such system involves the use of hyperfine states of ^{87}Rb atoms, specifically $F = 1, m_F = -1$ and $F = 2, m_F = 1$, which form a two-level atom system. Such a system of collection of indistinguishable atoms can be implemented using either hot or cold atomic ensembles or BECs [85]. To prepare two atomic systems in the entangled state, QND measurements are employed depending on the photonic detection outcomes. QND measurements have proven to be an effective method for inducing entanglement generation between atomic ensembles [34,63]. The QND scheme that we employ features a remarkably versatile geometry, enabling the measurement of physical qubits using addressable optical modes. With the Mach-Zehnder configuration, we can achieve entanglement between highly separated qubits, even when the line of sight is obstructed. This unique capability enhances the potential for robust and scalable entanglement generation. In Sec. II, we have summarized the formalism required to realize the QND measurement operator. For a particular QND measurement, the outcome is a random state and a sequence of QND pulses leads to a stochastic evolution of the system. By applying the conditional unitary operations, the desired state corresponding to the particular measurement outcome can be generated. The conditional unitary rotations are controlled by resonantly driving the transitions between the two states using a laser of appropriate resonant frequency.

VIII. SUMMARY AND CONCLUSIONS

In this paper we have introduced an adaptive QND scheme to generate the MMES between two atomic ensembles. The state is equivalent to a singlet state formed from two macroscopic spins, with total angular momentum zero, up to a local basis transform. Using the basic properties of the singlet state, we have proposed a protocol that can be implemented using QND measurements with adaptive unitary corrections and converges towards the MMES in a deterministic way. Our scheme is experimentally viable in the sense that it does not use complex operations such as transformations on individual atoms and only involves collective spin operations, projective measurements, and local unitary rotations. To check the efficiency of the scheme so as to converge the system towards MMES, we have calculated the fidelity, and the success probability to achieve target state after multiple rounds of measurements and corrections in a sequence. We observe that the probability and fidelity of obtaining the desired state increases in subsequent measurements. We have also checked the probability distribution of the measured state in Fock space and confirmed that it matches with spin correlations of the MMES.

Maximally entangled states find number of important applications in quantum information tasks as these serve as resource states for various quantum protocols. In Ref. [63], generation of two-mode squeezed states (TMSSs) was demonstrated under Holstein-Primakoff short interaction time regime in two separate gas cells. Here it is important to

understand the difference between TMSS and MMES. The amount of entanglement, as calculated by von Neumann entropy, in a TMSS is $\cosh^2 r \log_2(\cosh^2 r) - \sinh^2 r \log_2(\sinh^2 r)$, [71,86], where r is the squeezing parameter. Typically the squeezing parameter is in the region of $r \approx 1$, hence the amount of entanglement is of the order unity [29,63]. Meanwhile, the value for a MMES between two ensembles of dimension N is $\log_2(N + 1)$ [59]. This illustrates that the MMES possesses much more entanglement than in the TMSS. Moreover, in the MMES, the linear combination of all spin observables show correlations (or anticorrelations) [86], while in TMSS, only few spin observables are correlated (or anticorrelated). Our work provides a simple yet powerful method for producing a MMES and improves upon previous methods [77,91], which rely upon postselection. In addition, we have not preformed any approximation to spin variables in our calculations and have considered the spins in an exact way. The protocol works regardless of the initial state but we have considered the state that has the largest fidelity with the MMES, namely two spin coherent states polarized in the x direction.

An important topic is how robust our scheme is in the presence of experimental imperfections. In Sec. VI we performed two such case studies, of starting in a completely mixed state, and studying the effect of atomic number fluctuations. We have found that our scheme is very robust and converges to the MMES despite the presence of imperfections. In addition to this, we have made several studies of the effects of QND measurements under decoherence previously [92–94], which gives positive expectations of the performance of the current scheme. We briefly comment on prospects in this regard. We first point out that QND measurements have been shown to be remarkably robust against photon loss. In a previous work, decoherence effects on QND measurements were studied and shown that as long as the QND interaction times are in the short-time regime (as is the case with the measurements considered in this paper), decoherence on the atoms can be well-controlled [92].

Another technical challenge is the imperfect photonic resolution at the detectors. The primary effect of imperfect detector efficiency η is to reduce the average photon number α by an amount proportional to detection efficiency, i.e., $\alpha \rightarrow \alpha\sqrt{\eta}$, and modify the photon counts n_c, n_d in Eq. (9). Under such a replacement, the general form of Eq. (9) remains, however, of the same form, which suggests that the impact on entanglement generation itself may be small. In practice such imperfect photon detection may introduce further noise [93], but the robustness in our scheme is provided by the fact that only $\Delta = 0$ is the convergence point. This corresponds

to $n_d = 0$ according to Eq. (9), and the precise value of n_c itself does not matter. Hence, as long as the phase in the interferometer is unaffected, the imperfect photonic detection at the n_c detector does not affect the protocol. In the case of experimental realization with a bright laser source, limited photon-number resolution therefore should not significantly affect the fixed point at $n_d = 0$ and hence the convergence to the maximally entangled state is still expected to take place. The critical part of the protocol is to effectively distinguish the single measurement outcome at $n_d = 0$ from other possible outcomes. As shown in Sec. VIB, the protocol is not extremely sensitive to the particular rotation that is performed for $\Delta \neq 0$, and affects the convergence speed moderately but not the asymptotic state.

Another potential source of decoherence is the spontaneous emission of photons by the atoms. Since the QND interaction is a second-order effect, spontaneous emission via photon emission of the excited state can be an eventual source of dephasing of the atomic states [92]. We note, however, that the MMES is in fact not the most sensitive state to dephasing by its nature [59]. Other types of entangled states such as Bell states composed of Schrödinger cat states are much more sensitive to dephasing and we expect such states are poor candidates for experimental realization. On the other hand, the MMES as we consider here scales much better with the system size, and are a much more realistic prospect for experimental realization. In a controlled experiment, where the detuning is large, effects arising from spontaneous emission can be controlled to be a small quantity. In summary, we consider the most critical threat to experimental realization of the MMES is the atomic dephasing that QND measurements induce. However, this can be controlled, and with a careful choice of parameters, we believe dephasing effects can be minimized.

ACKNOWLEDGMENTS

This work is supported by the National Natural Science Foundation of China (62071301); NYU-ECNU Institute of Physics at NYU Shanghai; the Joint Physics Research Institute Challenge Grant; the Science and Technology Commission of Shanghai Municipality (19XD1423000, 22ZR1444600); the NYU Shanghai Boost Fund; the China Foreign Experts Program (G2021013002L); the NYU Shanghai Major-Grants Seed Fund; Tamkeen under the NYU Abu Dhabi Research Institute Grant No. CG008; Shanghai Frontiers Science Center of Artificial Intelligence and Deep Learning; and the SMEC Scientific Research Innovation Project (2023ZKZD55).

APPENDIX: EXPRESSION FOR TRANSFORMATION OF FOCK STATES THROUGH SPIN ROTATION

The Fock states $|k\rangle$ are eigenstates of the S^z spin operator, one can transform it to an arbitrary direction $|k\rangle^{(\theta, \phi)}$ as defined in Ref. [85] where the matrix elements of the S^y rotation are given by

$$\langle k' | e^{-iS^y \theta/2} | k \rangle = \sqrt{k!(N-k)!k'!(N-k')!} \sum_{n=\max(k'-k, 0)}^{\min(k', N-k)} \frac{(-1)^n \cos^{k'-k+N-2n}(\theta/2) \sin^{2n+k-k'}(\theta/2)}{(k'-n)!(N-k-n)!n!(k-k'-n)!}, \quad (\text{A1})$$

where $|k\rangle = |k\rangle^{(z)}$.

- [1] C. H. Bennett, G. Brassard, C. Crépeau, R. Jozsa, A. Peres, and W. K. Wootters, *Phys. Rev. Lett.* **70**, 1895 (1993).
- [2] C. H. Bennett, *Phys. Rev. Lett.* **68**, 3121 (1992).
- [3] T. D. Ladd, F. Jelezko, R. Laflamme, Y. Nakamura, C. Monroe, and J. L. O'Brien, *Nature (London)* **464**, 45 (2010).
- [4] N. D. Mermin, *Quantum Computer Science: An Introduction* (Cambridge University Press, New York, 2007).
- [5] J. Preskill, [arXiv:1203.5813](https://arxiv.org/abs/1203.5813).
- [6] R. Horodecki, P. Horodecki, M. Horodecki, and K. Horodecki, *Rev. Mod. Phys.* **81**, 865 (2009).
- [7] E. Chitambar and G. Gour, *Rev. Mod. Phys.* **91**, 025001 (2019).
- [8] M. M. Wilde, *Quantum Information Theory* (Cambridge University Press, New York, 2013).
- [9] D. Bouwmeester and A. Zeilinger, *The Physics of Quantum Information* (Springer Berlin, Heidelberg, 2000), pp. 1–14.
- [10] W. P. Schleich, K. S. Ranade, C. Anton, M. Arndt, M. Aspelmeyer, M. Bayer, G. Berg, T. Calarco, H. Fuchs, E. Giacobino *et al.*, *Appl. Phys. B: Lasers Opt.* **122**, 130 (2016).
- [11] M. A. Nielsen and I. L. Chuang, *Quantum Computation and Quantum Information: 10th Anniversary Edition* (Cambridge University Press, New York, 2010).
- [12] Y. Chi, J. Huang, Z. Zhang, J. Mao, Z. Zhou, X. Chen, C. Zhai, J. Bao, T. Dai, H. Yuan *et al.*, *Nat. Commun.* **13**, 1 (2022).
- [13] F. Bouchard, R. Fickler, R. W. Boyd, and E. Karimi, *Sci. Adv.* **3**, e1601915 (2017).
- [14] H. J. Briegel and R. Raussendorf, *Phys. Rev. Lett.* **86**, 910 (2001).
- [15] P. Facchi, G. Florio, G. Parisi, and S. Pascazio, *Phys. Rev. A* **77**, 060304(R) (2008).
- [16] D. Su, I. Dhand, and T. C. Ralph, *Phys. Rev. A* **106**, 042614 (2022).
- [17] Y. Wang, Z. Hu, B. C. Sanders, and S. Kais, *Front. Phys.* **8**, 589504 (2020).
- [18] N. J. Cerf, M. Bourennane, A. Karlsson, and N. Gisin, *Phys. Rev. Lett.* **88**, 127902 (2002).
- [19] A. J. Scott, *Phys. Rev. A* **69**, 052330 (2004).
- [20] E. T. Campbell, *Phys. Rev. Lett.* **113**, 230501 (2014).
- [21] T. Vértesi, S. Pironio, and N. Brunner, *Phys. Rev. Lett.* **104**, 060401 (2010).
- [22] V. Srivastav, N. H. Valencia, W. McCutcheon, S. Leedumrongwatthanakun, S. Designolle, R. Uola, N. Brunner, and M. Malik, *Phys. Rev. X* **12**, 041023 (2022).
- [23] A. Omeran, H. Levine, A. Keesling, G. Semeghini, T. T. Wang, S. Ebadi, H. Bernien, A. S. Zibrov, H. Pichler, S. Choi *et al.*, *Science* **365**, 570 (2019).
- [24] C. Senko, P. Richerme, J. Smith, A. Lee, I. Cohen, A. Retzker, and C. Monroe, *Phys. Rev. X* **5**, 021026 (2015).
- [25] D.-S. Ding, W. Zhang, S. Shi, Z.-Y. Zhou, Y. Li, B.-S. Shi, and G.-C. Guo, *Light: Sci. Appl.* **5**, e16157 (2016).
- [26] M. Neeley, M. Ansmann, R. C. Bialczak, M. Hofheinz, E. Lucero, A. D. O'Connell, D. Sank, H. Wang, J. Wenner, A. N. Cleland *et al.*, *Science* **325**, 722 (2009).
- [27] M. Kues, C. Reimer, P. Roztocki, L. R. Cortés, S. Sciara, B. Wetzler, Y. Zhang, A. Cino, S. T. Chu, B. E. Little *et al.*, *Nature (London)* **546**, 622 (2017).
- [28] C. Zhang, J. F. Chen, C. Cui, J. P. Dowling, Z. Y. Ou, and T. Byrnes, *Phys. Rev. A* **100**, 032330 (2019).
- [29] S. Kotler, G. A. Peterson, E. Shojaaee, F. Lecocq, K. Cicak, A. Kwiatkowski, S. Geller, S. Glancy, E. Knill, R. W. Simmonds *et al.*, *Science* **372**, 622 (2021).
- [30] K. Hammerer, A. S. Sørensen, and E. S. Polzik, *Rev. Mod. Phys.* **82**, 1041 (2010).
- [31] M. D. Lukin, S. F. Yelin, and M. Fleischhauer, *Phys. Rev. Lett.* **84**, 4232 (2000).
- [32] A. Sørensen, L.-M. Duan, J. I. Cirac, and P. Zoller, *Nature (London)* **409**, 63 (2001).
- [33] J. Hald, J. L. Sørensen, C. Schori, and E. S. Polzik, *Phys. Rev. Lett.* **83**, 1319 (1999).
- [34] A. Kuzmich, L. Mandel, and N. P. Bigelow, *Phys. Rev. Lett.* **85**, 1594 (2000).
- [35] C. Gross, *J. Phys. B: At., Mol. Opt. Phys.* **45**, 103001 (2012).
- [36] V. Giovannetti, S. Lloyd, and L. Maccone, *Phys. Rev. Lett.* **96**, 010401 (2006).
- [37] V. Giovannetti, S. Lloyd, and L. Maccone, *Science* **306**, 1330 (2004).
- [38] G. Tóth and I. Apellaniz, *J. Phys. A: Math. Theor.* **47**, 424006 (2014).
- [39] V. Giovannetti, S. Lloyd, and L. Maccone, *Nat. Photon.* **5**, 222 (2011).
- [40] C. You, S. Adhikari, Y. Chi, M. L. LaBorde, C. T. Matyas, C. Zhang, Z. Su, T. Byrnes, C. Lu, J. P. Dowling *et al.*, *J. Opt.* **19**, 124002 (2017).
- [41] H. Bao, J. Duan, S. Jin, X. Lu, P. Li, W. Qu, M. Wang, I. Novikova, E. E. Mikhailov, K.-F. Zhao *et al.*, *Nature (London)* **581**, 159 (2020).
- [42] P. Sekatski, M. Skotiniotis, J. Kołodyński, and W. Dür, *Quantum* **1**, 27 (2017).
- [43] J. S. Bell, *Phys. Phys. Fiz.* **1**, 195 (1964).
- [44] S. J. Freedman and J. F. Clauser, *Phys. Rev. Lett.* **28**, 938 (1972).
- [45] A. Aspect, J. Dalibard, and G. Roger, *Phys. Rev. Lett.* **49**, 1804 (1982).
- [46] G. Adesso, T. R. Bromley, and M. Cianciaruso, *J. Phys. A: Math. Theor.* **49**, 473001 (2016).
- [47] Z.-H. Ma, J. Cui, Z. Cao, S.-M. Fei, V. Vedral, T. Byrnes, and C. Radhakrishnan, *Europhys. Lett.* **125**, 50005 (2019).
- [48] R. Schmied, J.-D. Bancal, B. Allard, M. Fadel, V. Scarani, P. Treutlein, and N. Sangouard, *Science* **352**, 441 (2016).
- [49] J. Kitzinger, X. Meng, M. Fadel, V. Ivannikov, K. Nemoto, W. J. Munro, and T. Byrnes, *Phys. Rev. A* **104**, 043323 (2021).
- [50] A. Einstein, B. Podolsky, and N. Rosen, *Phys. Rev.* **47**, 777 (1935).
- [51] N. D. Mermin, *Rev. Mod. Phys.* **65**, 803 (1993).
- [52] K. Mattle, H. Weinfurter, P. G. Kwiat, and A. Zeilinger, *Phys. Rev. Lett.* **76**, 4656 (1996).
- [53] M. Żukowski, A. Zeilinger, M. A. Horne, and A. K. Ekert, *Phys. Rev. Lett.* **71**, 4287 (1993).
- [54] J. L. O'Brien, A. Furusawa, and J. Vučković, *Nat. Photon.* **3**, 687 (2009).
- [55] D. Sych and G. Leuchs, *New J. Phys.* **11**, 013006 (2009).
- [56] A. Cabello, *Phys. Rev. Lett.* **89**, 100402 (2002).
- [57] Y.-H. Luo, H.-S. Zhong, M. Erhard, X.-L. Wang, L.-C. Peng, M. Krenn, X. Jiang, L. Li, N.-L. Liu, C.-Y. Lu *et al.*, *Phys. Rev. Lett.* **123**, 070505 (2019).
- [58] X.-M. Hu, C. Zhang, B.-H. Liu, Y. Cai, X.-J. Ye, Y. Guo, W.-B. Xing, C.-X. Huang, Y.-F. Huang, C.-F. Li *et al.*, *Phys. Rev. Lett.* **125**, 230501 (2020).

- [59] T. Byrnes, *Phys. Rev. A* **88**, 023609 (2013).
- [60] Y. Jing, M. Fadel, V. Ivannikov, and T. Byrnes, *New J. Phys.* **21**, 093038 (2019).
- [61] M. Fadel, B. Yadin, Y. Mao, T. Byrnes, and M. Gessner, *New J. Phys.* **25**, 073006 (2023).
- [62] G. Vitagliano, M. Fadel, I. Apellaniz, M. Kleinmann, B. Lücke, C. Klempt, and G. Tóth, *Quantum* **7**, 914 (2023).
- [63] B. Julsgaard, A. Kozhekin, and E. S. Polzik, *Nature (London)* **413**, 400 (2001).
- [64] J. Esteve, C. Gross, A. Weller, S. Giovanazzi, and M. Oberthaler, *Nature (London)* **455**, 1216 (2008).
- [65] P. Kunkel, M. Prüfer, H. Strobel, D. Linnemann, A. Frölian, T. Gasenzer, M. Gärttner, and M. K. Oberthaler, *Science* **360**, 413 (2018).
- [66] M. Fadel, T. Zibold, B. Décamps, and P. Treutlein, *Science* **360**, 409 (2018).
- [67] P. Colciaghi, Y. Li, P. Treutlein, and T. Zibold, *Phys. Rev. X* **13**, 021031 (2023).
- [68] H. Krauter, D. Salart, C. Muschik, J. M. Petersen, H. Shen, T. Fernholz, and E. S. Polzik, *Nat. Phys.* **9**, 400 (2013).
- [69] A. N. Pyrkov and T. Byrnes, *New J. Phys.* **16**, 073038 (2014).
- [70] A. N. Pyrkov and T. Byrnes, *Phys. Rev. A* **90**, 062336 (2014).
- [71] S. L. Braunstein and P. van Loock, *Rev. Mod. Phys.* **77**, 513 (2005).
- [72] M. Chaudhary, M. Fadel, E. O. Ilo-Okeke, A. N. Pyrkov, V. Ivannikov, and T. Byrnes, *Phys. Rev. A* **103**, 062417 (2021).
- [73] E. O. Ilo-Okeke, L. Tessler, J. P. Dowling, and T. Byrnes, *npj Quantum Inf.* **4**, 40 (2018).
- [74] T. Byrnes, K. Wen, and Y. Yamamoto, *Phys. Rev. A* **85**, 040306(R) (2012).
- [75] T. Byrnes, D. Rosseau, M. Khosla, A. Pyrkov, A. Thomasen, T. Mukai, S. Koyama, A. Abdelrahman, and E. Ilo-Okeke, *Opt. Commun.* **337**, 102 (2015).
- [76] A. Abdelrahman, T. Mukai, H. Häffner, and T. Byrnes, *Opt. Express* **22**, 3501 (2014).
- [77] N. Behbood, F. Martin Ciurana, G. Colangelo, M. Napolitano, G. Tóth, R. J. Sewell, and M. W. Mitchell, *Phys. Rev. Lett.* **113**, 093601 (2014).
- [78] G. Tóth and M. W. Mitchell, *New J. Phys.* **12**, 053007 (2010).
- [79] N. Behbood, G. Colangelo, F. Martin Ciurana, M. Napolitano, R. J. Sewell, and M. W. Mitchell, *Phys. Rev. Lett.* **111**, 103601 (2013).
- [80] L. Balents, *Nature (London)* **464**, 199 (2010).
- [81] H. Cable and G. A. Durkin, *Phys. Rev. Lett.* **105**, 013603 (2010).
- [82] J. E. Aristizabal-Zuluaga, I. Skobleva, L. Richter, Y. Ji, Y. Mao, M. Kondappan, V. Ivannikov, and T. Byrnes, *J. Phys. B: At., Mol. Opt. Phys.* **54**, 105502 (2021).
- [83] M. Chaudhary, Y. Mao, M. Kondappan, A. S. P. Paz, V. Ivannikov, and T. Byrnes, *Phys. Rev. A* **105**, 022443 (2022).
- [84] L. Pezzè, A. Smerzi, M. K. Oberthaler, R. Schmied, and P. Treutlein, *Rev. Mod. Phys.* **90**, 035005 (2018).
- [85] T. Byrnes and E. O. Ilo-Okeke, *Quantum Atom Optics: Theory and Applications to Quantum Technology* (Cambridge University Press, UK, 2021).
- [86] J. Kitzinger, M. Chaudhary, M. Kondappan, V. Ivannikov, and T. Byrnes, *Phys. Rev. Res.* **2**, 033504 (2020).
- [87] M. Weissbluth, *Atoms and Molecules* (Elsevier, New York, 2012).
- [88] Y. Mao, M. Chaudhary, M. Kondappan, J. Shi, E. O. Ilo-Okeke, V. Ivannikov, and T. Byrnes, *Phys. Rev. Lett.* **131**, 110602 (2023).
- [89] M. Kondappan, M. Chaudhary, E. O. Ilo-Okeke, V. Ivannikov, and T. Byrnes, *Phys. Rev. A* **107**, 042616 (2023).
- [90] M. A. Kristensen, M. B. Christensen, M. Gajdacz, M. Iglicki, K. Pawłowski, C. Klempt, J. F. Sherson, K. Rzażewski, A. J. Hilliard, and J. J. Arlt, *Phys. Rev. Lett.* **122**, 163601 (2019).
- [91] N. Behbood, F. Martin Ciurana, G. Colangelo, M. Napolitano, M. W. Mitchell, and R. J. Sewell, *Appl. Phys. Lett.* **102**, 173504 (2013).
- [92] S. Gao, E. O. Ilo-Okeke, Y. Mao, M. Kondappan, J. E. Aristizabal-Zuluaga, V. Ivannikov, and T. Byrnes, *J. Phys. B: At., Mol. Opt. Phys.* **55**, 195501 (2022).
- [93] E. Ilo-Okeke and T. Byrnes (unpublished).
- [94] S. Gao, S. Li, M. Chaudhary, M. Prest, E. O. Ilo-Okeke, V. Ivannikov, and T. Byrnes, [arXiv:2302.13062](https://arxiv.org/abs/2302.13062).